CENTRAL STABLE/UNSTABLE MANIFOLDS AND THE DESTRUCTION OF KAM TORI IN THE PLANAR HILL PROBLEM

*C. SIMÓ
Departament de Matemàtica Aplicada i Anàlisi
Universitat de Barcelona, Barcelona, Spain.

AND

**T. J. STUCHI
Instituto de Física, Universidade Federal do Rio de Janeiro,
Rio de Janeiro, Brazil.

Abstract.

The classical Hill's problem is a simplified version of the restricted three body problem (RTBP) where the distance of the two massive bodies (say, primary for the largest one and secondary for the smallest) is made infinity through the use of Hills variables and a limiting procedure, so that a neighborhood of the secondary can be studied in detail. In this way it is the zeroth–order approximation in powers of $\mu^{1/3}$. The Levi–Civita regularization takes the Hamiltonian into the form of two uncoupled harmonic oscillators perturbed by the Coriolis force and the Sun action, polynomials of degree four and six, respectively.

As it is well known the RTBP has five equilibrium points, two triangular, L_4 and L_5, and three collinear, L_1, L_2 and L_3. In the Hill's version only two of the collinear, L_1 and L_2, remain and they are symmetric with respect to the secondary. The zero velocity curves (*zvc*) have a closed component, implying that the motion is bounded, only up to the energy value of these two libration points. For values of the energy larger than the one at L_1 and L_2 the *zvc* are open, and persistence of confined motion in that case is our main concern in this paper. We investigate the geometrical behavior of the center–stable and center–unstable manifolds of the libration points L_1 and L_2. Suitable Poincaré sections make apparent the relation between these manifolds and the main periodic orbits and also the destruction of the invariant KAM tori surrounding the secondary.

1. Introduction

The classical Hill's problem is a limit version of the restricted three body problem (RTBP). In this paper we shall focus on the planar case. A change of scale depending on the mass ratio μ, and more concretely on $\mu^{1/3}$, allows to write the Hamiltonian of the RTBP in a $O(\mu^{1/3})$–neighborhood of the secondary as a power series in $\mu^{1/3}$. Letting μ go to 0 gives a limit problem. This is, precisely, Hill's problem. In this way the mass of the secondary is scaled to 1, the primary is sent to an infinite distance, the mass increasing also to infinity, so that his action is a force field on a given direction. Furthermore one has also a Coriolis force due to the use of a rotating frame.

Then, Levi–Civita regularization is used to obtain a polynomial Hamiltonian which is very convenient for numerical calculations. Also it conveys a more general framework for many readers of other areas than Celestial Mechanics.

The polynomial Hamiltonian for the regularized Hill's problem takes the form of two uncoupled harmonic oscillators with the same frequency (which is the translation to these variables of Kepler's problem) perturbed by polynomial terms. The fourth degree terms are due to the Coriolis force since we have changed the inertial reference frame in the center of mass to a rotating frame (synodical) centered in the secondary. Up to this order the Hamiltonian is integrable. The sixth degree terms, due to the action of the primary, turn the problem non integrable. However the authors are not aware of any analytical proof of this fact for the planar case.

As it is well known the L_1 and L_2 equilibrium points are saddle–centers. Associated to the imaginary eigenvalues there is a center manifold foliated by symmetric periodic orbits known as Lyapunov orbits. These orbits can be obtained analytically by the classical Lindstedt–Poincaré method or by numerical continuation. From these orbits we obtain, through numerical globalization, the center–unstable (stable) manifolds of L_1 and L_2. In fact, due to the symmetries of the Hamiltonian we need to determine just one of these manifolds and apply the symmetry to obtain the others. A convenient Poincaré section shows the relation of these manifolds and the remaining KAM structure when the energy is increased. The geometrical relation between this structure and the center–stable/unstable manifolds is our main concern in this paper.

In section 2 we present the equations of motion and the regularized version. Some general features, the local behavior around the saddle–centers and Poincaré sections are presented in section 3. The numerically determined Lyapunov orbits and other periodic orbits are discussed in section 4. The globalization of the center–stable/unstable manifolds is described in section 5 together with the Poincaré sections of both these manifolds and invariant KAM tori. Some conclusions and outlook are presented at the end.

2. The Hill's Hamiltonian and its regularization

2.1. FROM THE PLANAR RTBP TO HILL'S HAMILTONIAN

Let P_1 and P_2 be the primary and secondary with masses $m_1 = 1 - \mu$ and $m_2 = \mu$, $\mu < 1/2$, respectively, describing circular orbits due to the their mutual gravitational attraction only. In a rotating system of coordinates, with origin at the center of mass, Newton's equations for a massless particle P_0, which does not disturb the motion of P_1 and P_2, are

$$\begin{aligned} \ddot{x} - 2\dot{y} &= x - \frac{(1-\mu)\,(x-\mu)}{r_1^3} - \frac{\mu(x+1-\mu)}{r_2^3}\,, \\ \ddot{y} + 2\dot{x} &= y\left(1 - \frac{1-\mu}{r_1^3} - \frac{\mu}{r_2^3}\right)\,, \end{aligned} \tag{1}$$

where $r_1^2 = (x-\mu)^2 + y^2$ and $r_2^2 = (x-\mu+1)^2 + y^2$ as shown in Figure 1. The positions of the bodies are $P_1 = (\mu, 0)$ and $P_2 = (1-\mu, 0)$.

Note that these coordinates are dimensionless, i.e., the unit of mass is $m_1 + m_2 = 1$, the unit of length is the distance between P_1 and P_2 and the unit of time is chosen in

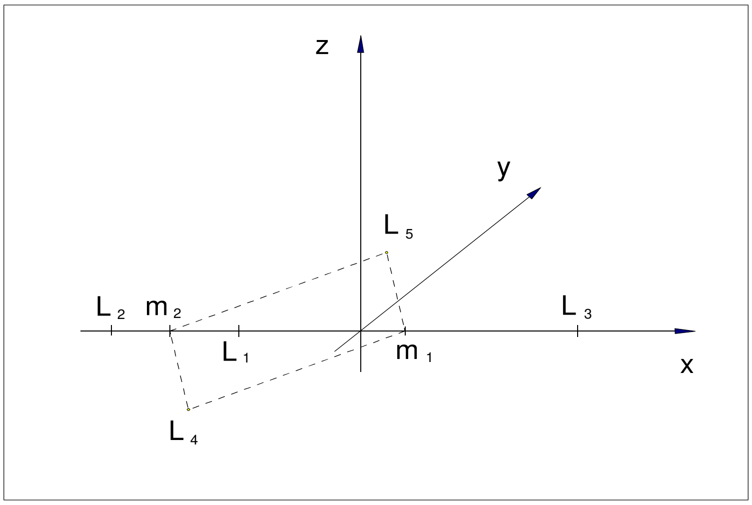

Figure 1. The setup of the restricted three body problem (spatial in this figure).

order to make the period of revolution of the primaries equal to 2π. In these units the gravitational constant, G, is taken equal to 1 . Equations (1) for the planar RTBP have a first integral, namely the Jacobi integral, with the following expression:

$$\mathcal{C}_{\mathcal{J}} = -\left(\dot{x}^2 + \dot{y}^2\right) + 2\,\Omega\,(x, y)\ , \tag{2}$$

where

$$\Omega\,(x, y) = \frac{(x^2 + y^2)}{2} + \frac{1-\mu}{r_1} + \frac{\mu}{r_2} + \frac{1}{2}\mu\,(1-\mu)\,, \tag{3}$$

is the gravitational potential in synodic coordinates. The constant term in (3) is chosen so that using (2) one has $\mathcal{C}_{\mathcal{J}} = 3$ at L_4 and L_5 .

We now make Hill's transformation which consists of a translation to the secondary followed by a rescaling, namely

$$x = X\mu^{1/3} + \mu - 1, \quad \dot{x} = \dot{X}\mu^{1/3}, \quad y = Y\mu^{1/3}, \quad \dot{y} = \dot{Y}\mu^{1/3} \tag{4}$$

and expand $\mathcal{C}_{\mathcal{J}}$ in powers of $\mu^{1/3}$. Some leading terms cancel, and the dominant terms which remain give the Hill limit. Using (4) the expansion takes the following form:

$$C_H = -\dot{X}^2 - \dot{Y}^2 + \frac{2}{(X^2+Y^2)^{1/2}} + 3X^2 + \mu^{1/3}(2X^3 - 3XY^2) + \\ + \mu^{2/3}(2X^4 - 6X^2Y^2 + \frac{3}{4}Y^4) + O(\mu),$$

where $C_H = \mu^{-2/3}(\mathcal{C}_{\mathcal{J}} - 3(1-\mu))$, and $\mu^{2/3}C_H \to \mathcal{C}_{\mathcal{J}} - 3$ as μ goes to zero.

The Hamiltonian function for the term independent of μ is:

$$H_H(q_1, q_2, p_1, p_2) = \frac{1}{2}(p_1^2 + p_2^2) - \frac{1}{(q_1^2+q_2^2)^{1/2}} + q_2p_1 - q_1p_2 - q_1^2 + \frac{1}{2}q_2^2, \tag{5}$$

where $q_1 = X$, $q_2 = Y$, $p_1 = \dot{X} - Y$ and $p_2 = \dot{Y} + X$ are a canonical set of variables. The relation between this Hamiltonian and C_H is $H = -C_H/2$. We now clearly see a Kepler problem perturbed by the Coriolis force and the action of the Sun up to zeroth–order of $\mu^{1/3}$. So Hill's model is the first approximation to the RTBP appropriate for studying the neighborhood of the secondary and which takes into consideration the action of the primary. The next two terms in the expansion are

$$H_{1/3} = -2q_1^3 + 3q_1q_2^2, \quad H_{2/3} = -2q_1^4 + 6q_1^2q_2^2 - \frac{3}{4}q_2^4 .$$

Perhaps it is worthwhile to note that this model applied to the motion of the Moon gives a good description of its actual orbit and therefore justifies this approximation to the RTBP in the neighborhood of the secondary (the Earth, the primary being the Sun). It is also useful to gain insight on the complete RTBP since some phenomena can be guessed by analyticity with respect to $\mu^{1/3}$.

2.2. LEVI–CIVITA REGULARIZATION

We now apply the following change of variables $\mathbf{L}(\hat{\mathbf{q}})$, $\hat{\mathbf{q}} = (\hat{q}_1, \hat{q}_2)$, known as Levi–Civita transformation, given by:

$$\begin{pmatrix} q_1 \\ q_2 \end{pmatrix} = \begin{pmatrix} \hat{q}_1 & -\hat{q}_2 \\ \hat{q}_2 & \hat{q}_1 \end{pmatrix} \begin{pmatrix} \hat{q}_1 \\ \hat{q}_2 \end{pmatrix}, \tag{6}$$

the induced conjugate momenta transformation being

$$\begin{pmatrix} p_1 \\ p_2 \end{pmatrix} = \frac{2}{(\hat{r}^2)} \begin{pmatrix} \hat{q}_1 & -\hat{q}_2 \\ \hat{q}_2 & \hat{q}_1 \end{pmatrix} \begin{pmatrix} \hat{p}_1 \\ \hat{p}_2 \end{pmatrix}, \tag{7}$$

where $\hat{r}^2 = (\hat{q}_1^2 + \hat{q}_2^2) = r = (q_1^2 + q_2^2)^{1/2}$. To complete the regularizing procedure it is also necessary a change of time scale, given by

$$d\tau = \frac{4\ dt}{(\hat{q}_1^2 + \hat{q}_2^2)} \tag{8}$$

Using (6), (7) and (8) in (5), the corresponding Hamiltonian, $\hat{H}(\hat{\mathbf{q}}, \hat{\mathbf{p}}) = \frac{r}{4}(H_H(\hat{\mathbf{q}}, \hat{\mathbf{p}}) + p_0)$, where the hat has been suppressed from the variables is

$$H = \left(\frac{p_0}{2}\right) \frac{(q_1^2 + q_2^2)}{2} + \frac{1}{2}(p_1^2 + p_2^2) + \frac{1}{2}(q_1^2 + q_2^2)(q_2p_1 - q_1p_2) - \frac{1}{4}(q_1^6 - 3q_1^4q_2^2 - 3q_1^2q_2^4 + q_2^6), \tag{9}$$

where $\frac{p_0}{2} = \frac{-h_H}{2} = c_H/4 = c$, c_H and h_H being the values of C_H and H_H, the Hill's Jacobian constant and the nonregularized Hamiltonian, respectively. Note that c has the same sign as the Jacobi's constant and the opposite sign of the non–regularized Hamiltonian.

The regularized Hamiltonian (9) is still dependent on the parameter c which is eliminated through the canonical change of variables given by

$$q_1 = \alpha Q_1, \quad q_2 = \alpha Q_2, \quad p_1 = \beta P_1, \quad p_2 = \beta P_2, \tag{10}$$

and $H = \gamma\mathcal{H}$, where $\alpha = 2c^{1/4}$, $\beta = 2c^{3/4}$ and $\gamma = c^{-3/2}/4$. Note that we assume implicitely here that $c > 0$. We shall be mainly interested in that case, because the libration points and their vicinity are on that region. Furthermore, when c goes to 0 then h (the value of the new Hamiltonian) goes to ∞ and viceversa. Anyway, when one is interested in negative values of c just take the same scaling using $|c|$. The suitable modifications of the Hamiltonian will be detailed later. Obviously, the scale does not apply when $c = 0$.

We are finally left with a Hamiltonian without any parameter which will be used for our numerical work in the next sections. It can be decomposed into homogeneous components

$$H(Q_1, Q_2, P_1, P_2) = H_2 + H_4 + H_6, \tag{11}$$

where

$$\begin{aligned} H_2 &= \tfrac{1}{2}(Q_1^2 + Q_2^2 + P_1^2 + P_2^2), \\ H_4 &= 2({Q_1}^2 + {Q_2}^2)(Q_2 P_1 - Q_1 P_2), \\ H_6 &= -4({Q_1}^6 + {Q_2}^6 - 3{Q_1}^4{Q_2}^2 - 3{Q_1}^2{Q_2}^4) \end{aligned} \tag{12}$$

and the equations of motion are:

$$\begin{aligned} \dot{Q}_1 &= P_1 + 2RQ_2, \\ \dot{Q}_2 &= P_2 - 2RQ_1, \\ \dot{P}_1 &= -Q_1 + 2RP_2 - 4Q_1F_c + 24Q_1(Q_1^4 - 2Q_1^2Q_2^2 - Q_2^4), \\ \dot{P}_2 &= -Q_2 - 2RP_1 - 4Q_2F_c + 24Q_2(Q_2^4 - 2Q_1^2Q_2^2 - Q_1^4), \end{aligned} \tag{13}$$

where $R = Q_1^2 + Q_2^2$ and $F_c = Q_2P_1 - Q_1P_2$ (the Coriolis force). In the case of negative $c = c_H/4$, just take its modulus and change the sign of the harmonic oscillator potential (i.e., H_2 should be $\frac{1}{2}(-Q_1^2 - Q_2^2 + P_1^2 + P_2^2)$). Care should be taken since c and $-c$ correspond to the same value of h, but they are not the same Hamiltonian system. The case with $c = 0$ has to be dealt using Hamiltonian (9) without scaling and leaving off the harmonic oscillator potential (i.e., H_2 should be $\frac{1}{2}(P_1^2 + P_2^2)$).

In this regularized Hill Hamiltonian, as mentioned before, H_2 is the Kepler term and H_4 is the Coriolis one. $H_2 + H_4$ is integrable in the Liouville–Arnold sense. The remaining term, H_6, is the perturbative action of the primary. Integrability breaks down under this term, i.e., invariant tori are deformed or destroyed according to the well–known results of KAM theory. The simple expressions in (12) and (13) make computations easier.

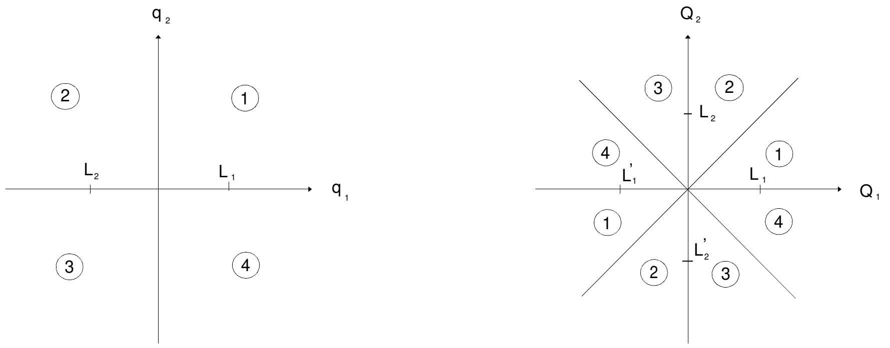

Figure 2. The original canonical (left) and the Levi–Civita (right) variables for the positions. The original fixed points L_1 and L_2 are now in the positive horizontal and vertical axes, respectively.

The Levi–Civita transformation makes a double covering. Therefore, L_1 and L_2 are the images of the previous points under this transformation, while L_1' and L_2' are copies of the former. It is convenient to note that the Levi–Civita transformation doubles angles around the origin, while distances are related by the square root (see (6), (7) and Figure 2). The symmetries of the original problem are enlarged in the regularized version and will be fully discussed in section 5.

3. General features of Hill's problem

The above Hamiltonian has three equilibrium points, one center and two saddle–centers with the following coordinate values: in the non–regularized variables (q_1, q_2, p_1, p_2)

$$O \to (0,0,0,0), \quad L_1 \to (3^{-1/3}, 0, 0, 3^{-1/3}), \quad L_2 \to (-3^{-1/3}, 0, 0, -3^{-1/3})$$

and in LC variables (Q_1, Q_2, P_1, P_2)

$$L_1 \to (6^{-1/2}, 0, 0, 6^{-1/2}/3), \quad L_2 \to (0, 6^{-1/2}, 6^{-1/2}/3, 0),$$

$$L_1' \to (-6^{-1/2}, 0, 0, -6^{-1/2}/3), \quad L_2' \to (0, -6^{-1/2}, -6^{-1/2}/3, 0).$$

Obviously, the origin now is a regular point and still a center–center equilibrium point of the system (collision becomes an equilibrium because of the slow down change (6)). As already mentioned the transformation makes a double covering, so the number of equilibrium points is doubled.

In cartesian variables, the eigenvalues for L_1 and L_2 are $\bar{\lambda}_1 = i\bar{\omega} = i(-1+2\sqrt{7})^{1/2}$ and $\bar{\lambda}_2 = (1+2\sqrt{7})^{1/2}$, i.e., a center and a saddle, respectively. At these points the values of the Jacobian first integral and the Hamiltonian (11) are $c_h = 3^{4/3}$ and $h = \frac{1}{18}$, respectively. Note that the eigenvalues in the regularized version have new values (due to the change of time) given by: $\lambda_i = \frac{2}{3}\bar{\lambda}_i$ ($\lambda_1 = \pm i\ 1.38106$, $\lambda_2 = \pm 1.67219$). The relation between our Hamiltonian and Hill's Jacobi constant is $h = (|c_H|^{-3/2})/2$, $c_H \neq 0$, which clearly shows the singular nature of our scaling and also that c_H can be negative. So, in the numerical calculations care should be taken when c_H goes to zero, mainly when continuing families of periodic orbits.

Up to $h = 1/18$ we have one closed component of the *zvc*. From this value on we have Lyapunov periodic orbits which are, of course, unstable. In this case the existence of bounded motion can no longer be assured by using only topological constrains, and we shall show how the stable and unstable manifolds of the Lyapunov orbits interplay with this open structure of trajectories. So, we present now the local behavior followed by some preliminary numerical results.

3.1. LOCAL BEHAVIOR NEAR THE LIBRATION POINTS

As it is well known, Hamiltonian (11) translated to L_i and transformed to the real eigenvectors basis takes the form:

$$H(q_1, q_2, p_1, p_3) = \frac{\omega}{2}(q_1^2 + p_1^2) + \frac{\lambda_2}{2}(p_2^2 - q_2^2) + \sum_{|\mathbf{k}|+|\mathbf{l}|\geq 3} c_{\mathbf{kl}} \quad \mathbf{q}^{\mathbf{k}}\mathbf{p}^{\mathbf{l}}, \tag{14}$$

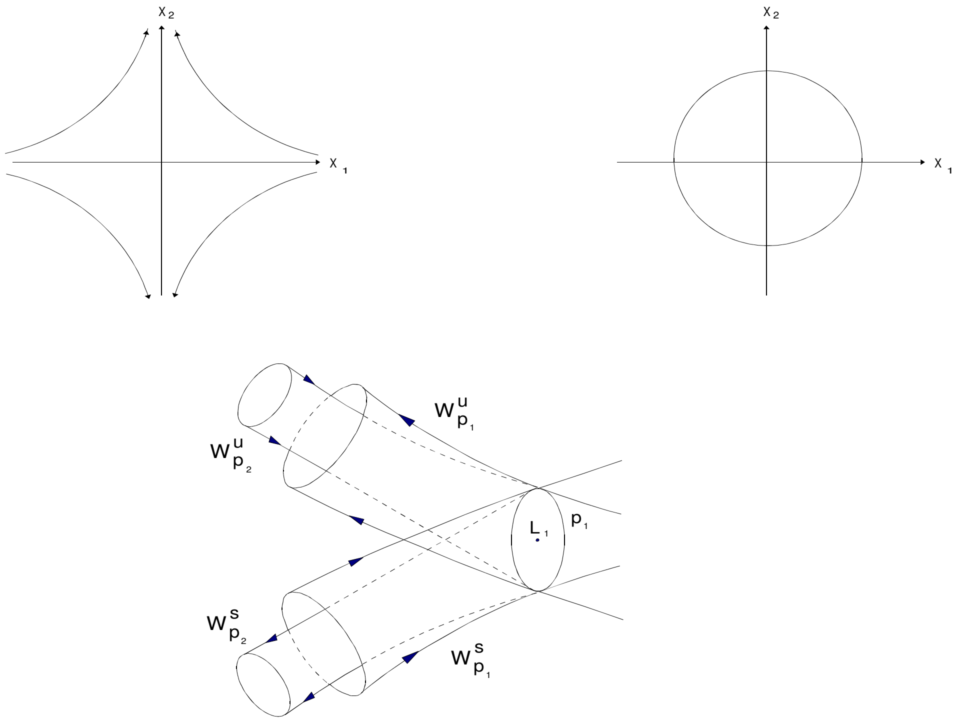

Figure 3. Linear dynamics around L_i. The top left shows the saddle part while the right one the center. At the bottom, an outlay of the invariant manifolds at a periodic orbit p_1 around L_1 showing also their counterpart coming from p_2 around L_2.

where $\mathbf{k}, \mathbf{l} \in (\mathbf{N} \cup \{0\})^2$, $|\mathbf{k}| = k_1 + k_2$ and $|\mathbf{l}| = l_1 + l_2$. There is a (complex) change of variables which takes Hamiltonian (14) to

$$H_q(x_1, x_2, y_1, y_2) = i\omega_1 x_1 y_1 - \lambda_2 x_2 y_2 + \sum_{|\mathbf{k}|+|\mathbf{l}| \geq 3} C_{\mathbf{kl}} \mathbf{x}^{\mathbf{k}} \mathbf{y}^{\mathbf{l}} \tag{15}$$

with $\mathbf{k}, \mathbf{l}$ as before, and we can express the quadratic part of (15) as :

$$H_q = H_c + H_s.$$

The expression in (15) is useful to obtain formal approximations to the center manifold. In the present case they are convergent.

In Figure 3, we try to illustrate the linear behavior of a neighborhood of the libration points. In the top drawings (x_1, x_2) means either (x_1, y_1) or (x_2, y_2). If $h_c = 0$ and $h = h_s = \lambda x_2 y_2 = 0$, then the axes $x_2 = 0$ and $y_2 = 0$ are the linear unstable and stable directions, respectively $W^U_{L_i}$ and $W^S_{L_i}$. If $h_s \neq 0$ we are on the hyperbolae near the stable/unstable manifolds of the equilibrium point (Figure 3 top left).

When $h = h_c \neq 0$, $h_s = 0$, if $x_2 = y_2 = 0$ we are restricted to the plane (x_1, y_1) where there is a family of unstable periodic orbits of the linear system. These periodic orbits generate the tangent plane to the center manifold. If now only $y_2 = 0$, then the motion is composed by the periodic orbit (p.o.) and the axis x_2. Two unstable semicylinders, $W^U_{p.o.}$, are then generated. The composition of the p.o. and y_2 gives rise to $W^S_{p.o.}$.

In the variables (x_i, y_i) or in the (q_i, p_i) when higher order terms are taken into account, the cylinders will appear distorted (Figure 3 bottom) but preserving the topology just described. Moreover, far away from the saddle–centers (L_i) the distortion can be such as to make them wander in complicated tangles. In our particular case if we allow to act as non–linear perturbation the Coriolis force only, the unstable (stable) cylinders from a given p.o. around L_1 will coincide with stable (unstable) cylinders of L_2, since this part of the system is integrable. However, if the full perturbation is to act, $W^U_{p.o.}$ and $W^S_{p.o.}$ will split and intersect each other generating homoclinic and/or heteroclinic orbits. The next numerical results show the KAM structure which in section 5 will be discussed together with the non–linear behavior of the manifolds whose linear behavior we have just illustrated.

3.2. PRELIMINARY NUMERICAL RESULTS

We find that a convenient Poincaré section is $Q_2 = 0$ ($\dot{Q}_2 > 0$). Of course, it is not a global Poincaré section, the flow being tangent to it at the boundary of the admissible domain. In subsequent figures we display, on this section, the Q_1 and P_1 coordinates. Figure 4 shows some of these sections going from lower to higher energy values for c_H positive. The orbits on the lefthand side are retrograde orbits. Of course, some orbits lying on tori (and seen on the figures as invariant curves) can have a part on the left and a small part on the right. They have, essentially, a retrograde character.

At $h = 0$ ($c_h \to \infty$) the origin is a fixed stable point. As c_H becomes finite through positive values, i.e., for low energy values, two stable fixed points appear on the Poincaré section. The one on the right corresponds to a Moon–like trajectory and it is direct. The lefthand side fixed point corresponds to retrograde lunar motion. As the energy increases the direct motion tori deform faster than the retrograde ones.

The rigth stable fixed point undergoes a pitchfork bifurcation at $h = 0.0523785$, so that there are now two stable Moon like trajectories and the former one becomes unstable. The pitchfork can be seen in Figure 5. The same bifurcation is shown in Figure 9 (cartesian variables) as the e–family. Note that it bifurcates before the *zvc* opens. The bifurcated families end up on collision and from this point on they can be continued if we allow for an extra loop. This will be discussed in more detail in the next section.

After the pitchfork bifurcation, the right region becomes more and more chaotic as h increases. In fact, letting aside the small islands corresponding to the bifurcated stable families, it is completely stochastic in the maple leaf shaped region displayed in Figure 4–c. All this happens before the *zvc* open and the Lyapunov orbits start to appear. Note how the number of iterates falls as we pass from Figure 4–c to 4–d, when the energy passes from $h = 0.0555$ to $h = 0.05558$, i.e., a not very large energy increase. However, after the *zvc* opens, some part of this chaotic zone starts to get organized again and some fairly large stability islands reappear on the right (Figure 4–e). Other points in the previous chaotic zone find the way to escape (see Figure 4–d to 4–f).

A peculiar set of periodic orbits is shown in Figure 6. Four periodic orbits with rotation number 1/3 which are seen as if they were a set of twelve islands. They correspond to the energy value $h = 0.0541$. Of course, this behavior can be theoretically created with the help of normal forms but it is interesting to find an example in such a classical problem as Hill's problem. This problem displays many bifurcations which are very far from generic, even if we take into account the symmetries. Figure 6 is just an example of this fact.

An interesting feature is shown by the fixed point of the Poincaré map on the left. It is strongly stable and as already mentioned it corresponds to retrograde moons. Numerical

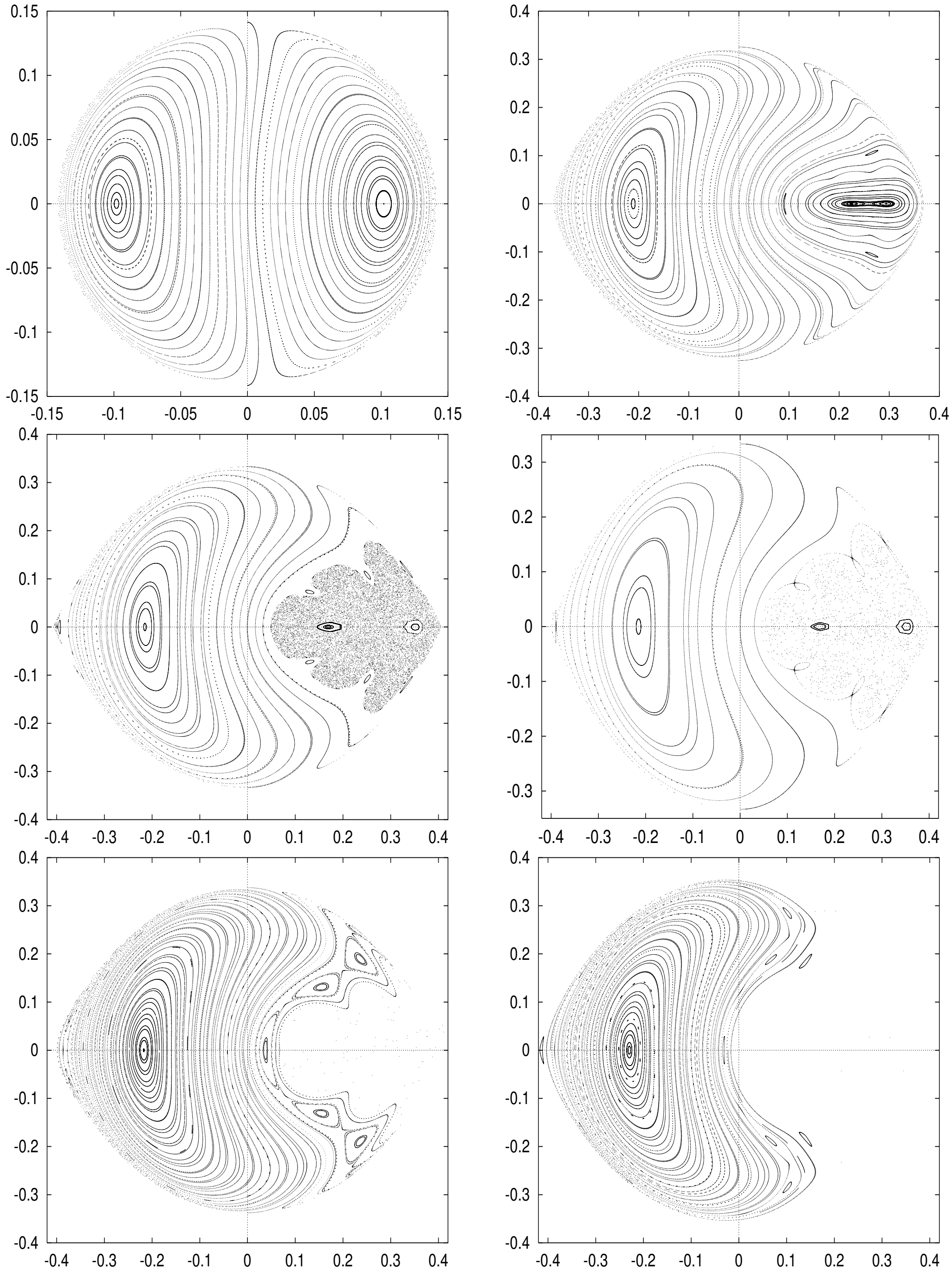

Figure 4. Poincaré section $Q_2 = 0$ (1000 iterates for several initial conditions). From left to right and from top to bottom: a) $h = 0.01$ ($c_H = 13.572089$); b) $h = 0.053$ ($c_H = 4.4647393$); c) $h = 0.0555$ ($c_H = 4.3296356$); d) $h = 0.05558$ ($c_H = 4.3254802$); e) $h = 0.057$ ($c_H = 4.2533402$) and f) $h = 0.065$ ($c_H = 3.8967671$). Iterates on the left part of each subfigure correspond to retrograde orbits.

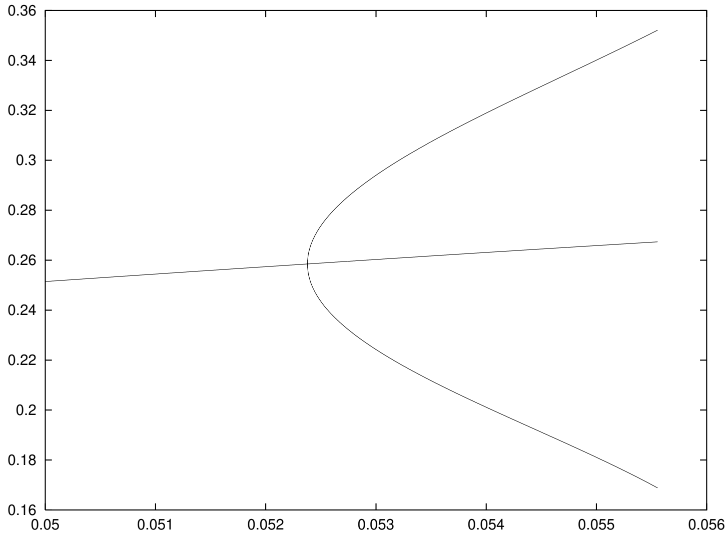

Figure 5. The pitchfork bifurcation at $h = 0.0523785$. So there are two initially stable Moon like trajectories and the former one is made unstable. See Figure 9, in physical variables, for more details.

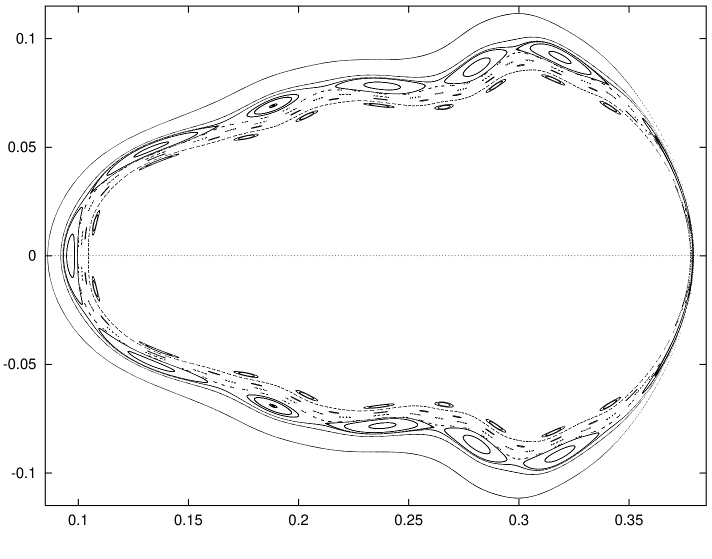

Figure 6. Four periodic orbits with rotation number 1/3 at $h = 0.0541$.

experiments show that it subsists for arbitrarily high negative values of the Jacobi constant. As c_H goes to 0^+, h goes to ∞, it crosses a 1 to 3 resonance (for $c_H = 0.0153884$, $h = 261.928$) and the triangular shape figure changes side after shrinking to zero. Note the changes in Figure 7–a, 7–b and 7–c, and the differences in scale. The inverted triangle continues growing until it crosses again a 1 to 3 resonance (for $c_H = -1.411618$, $h = 0.298122$), shrinks to zero and grows indefinitely as c_H goes to $-\infty$ (h goes to 0). Figure 7–e to 7–f show this behavior after the second crossing. The value $c_H = 0$ ($h \to \infty$) is a special value only from the point of view of our special scaling, otherwise no interesting feature occurs at it (see Figure 8).

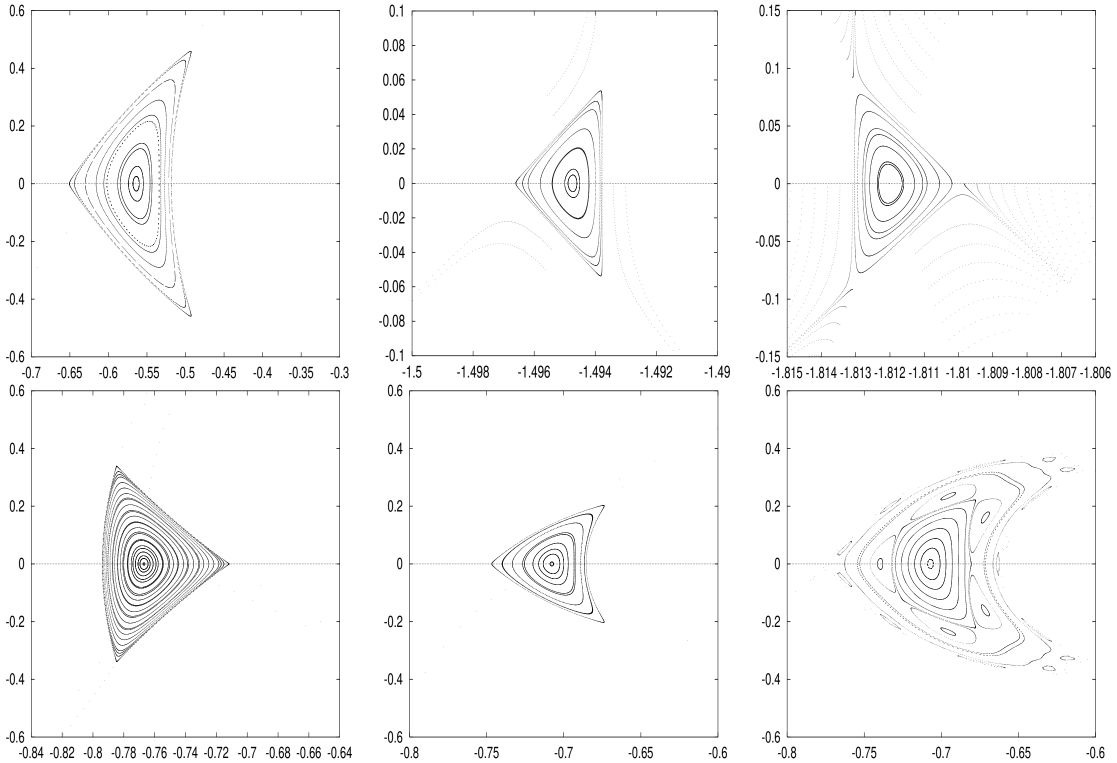

Figure 7. Poincaré section $Q_2 = 0$ (1000 iterates for several initial conditions) showing the retrograde strongly stable periodic orbits which appear on the left of Figure 4. From left to right and from top to bottom: a) $c_H = 0.62996052$ ($h = 1.0$); b) $c_H = 0.02137470$ ($h = 160$); c) $c_H = 0.01$ ($h = 500$); d) $c_H = -0.5$ ($h = 1.41421356$); e) $c_H = -2.0$ ($h = 0.17677670$) and f) $c_H = -4.0$ ($h = 0.0625$).

4. Lyapunov periodic orbits and other main periodic orbits

The RTBP, and in particular, its Hill limit problem has the following symmetry in both the cartesian synodical coordinates or in their canonical version

$$\begin{array}{l} S_1 : (x, y, \dot{x}, \dot{y}, t) \to (x, -y, -\dot{x}, -\dot{y}, -t) \\ S_2 : (q_1, q_2, p_1, p_2, t) \to (q_1, -q_2, -p_1, p_2, -t). \end{array} \tag{16}$$

This symmetry implies that the Lyapunov periodic orbits are symmetric with respect to the x or q_1 axis, the original cartesian and canonic coordinates respectively. A well known result states that if a trajectory crosses the axis of symmetry orthogonally at $t = 0$ and $t = T/2$ then the orbit is closed and of period T.

In general, to compute a T–periodic orbit of an autonomous system $\dot{x} = f(y)$, through x_0, means to find the zeros of the function $F(x_0) = \varphi(T, x_0) - x_0 = 0$, where $\varphi(t, x_0)$ is the solution starting at x_0 when $t = 0$. It is equivalent to deal with the problem of finding a fixed point of a Poincaré map $\mathcal{P}(x_0)$ of $\varphi(t, x_0)$ associated to a section Σ transversal to this flow. Given Σ and $\mathcal{P}(x_0)$ as above we have now to find $x_0 \in \Sigma$ such that

$$F(x_0) = (\varphi(t, x_0) \cap \Sigma) - x_0 = \mathcal{P}(x_0) - x_0 = 0. \tag{17}$$

Equation (17) can be transformed into a continuation problem through a homotopy. For details we refer to [4].

Consider the following set of initial conditions $(Q_1^0, 0, 0, P_2^0)$. This means that we are in the Poincaré section $Q_2 = 0$ $(H = h, \dot{Q}_2 > 0)$ and the orbit crosses the Q_1 axis orthogonally, i.e, $P_1 = 0$. We search the next crossing after one half turn where $P_1 = 0$ again. This is done using a predictor–corrector method to solve the continuation equation. As already mentioned, because of the symmetry of the periodic orbits we can reduce computational costs and integrate one half period only. The method is applied in regularized variables and the results can be transformed back to the synodic variables whenever desired through (6), (7), (8) and (10). As a consequence of the singular scale, we have in fact two Hamiltonian systems and care should be taken when continuing orbits through $c_H = 0$.

The orbits we obtain have already been determined by Hénon [1] as part of a series of numerical studies of the RTBP. However, no explicit conexion was made there between their invariant manifolds and the KAM structure.

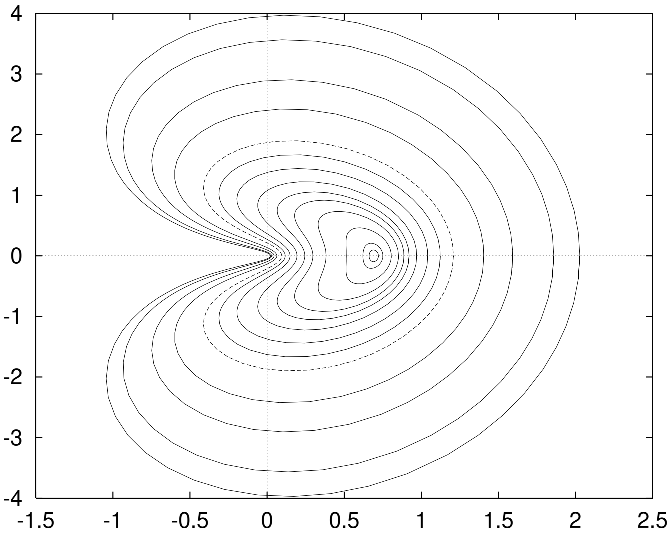

Figure 8. The (x, y) projections of some Lyapunov periodic orbits which form the center manifold of L_1. The ones for L_2 can be obtained by symmetry. They go asymptotically to collision as c_H goes to $-\infty$ $(h \to 0)$. The dashed Lyapunov orbit is for $c_H = 0$.

In Figure 8 we show some Lyapunov periodic orbits of L_1 projected in the (x, y) plane, i.e., in the cartesian physical variables. There is a one–parameter set of these orbits and they generate the center manifold associated to the libration points. As L_1 and L_2 are symmetric with respect to the Q_2 axis, the periodic orbits of L_2 are obtained from those of L_1 by symmetry. The dashed orbit is the Lyapunov orbit for $c_H = 0$ and as it was mentioned at end of last section it does not have any special feature. The four largest orbits are for negative c_H, namely, -0.51629634, -0.94984956, -1.5681896, and -1.9804931, while the four first ones to the right of the $c_H = 0$ one have the following values of the Jacobi constant: $c_H = 0.27707190, 0.61869355, 1.0537016$, and 1.5112690.

In Figure 9 we show the characteristic curves of some families of periodic orbits which, in the physical variables, close after one and two loops. The initial value of the physical variable x is shown in the vertical axis, while the value of c_H is shown in the horizontal one. The Lyapunov orbits, l_1 and l_2, start near L_1 and L_2, respectively, just after the *zvc* open; this happens for $c_H = 4.3267487$ $(h = \frac{1}{18})$. We have plotted always the left most crossing of the x-axis so that the span of the Lyapunov orbits can be estimated. As it can be seen in the figure they go asymptotically to collision as c_H goes to $-\infty$.

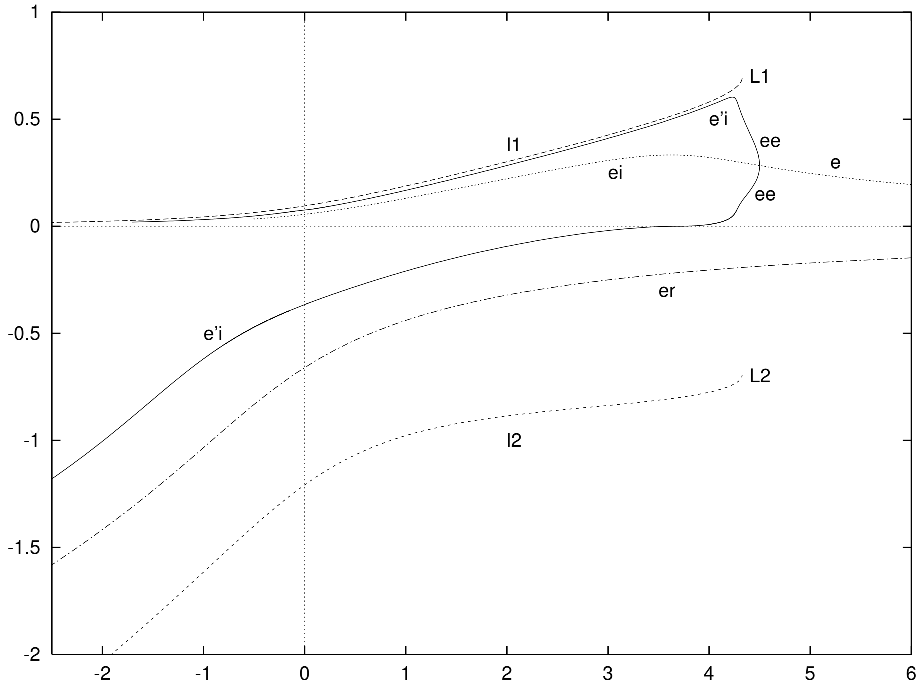

Figure 9. Some of the main periodic orbits of period one. The vertical axis is an initial or final condition of the periodic orbit generated by numerical continuation. The horizontal one is the value c_H of the Jacobi constant. Families l_1, l_2 and e go asymptotically to collision.

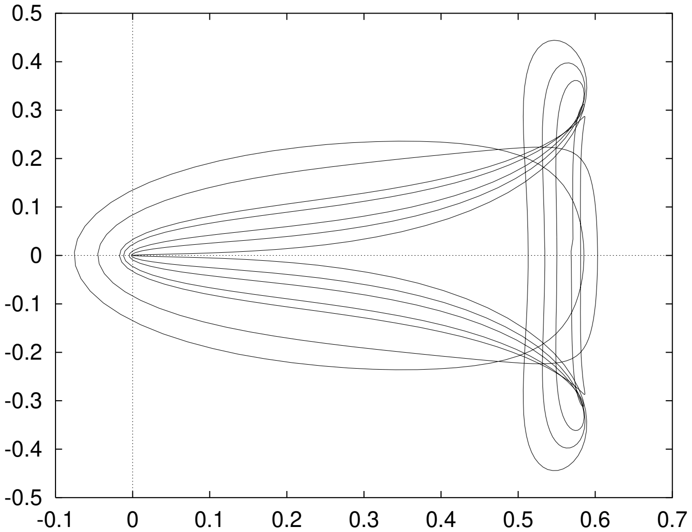

Figure 10. Some orbits of the $e'i$–family starting in the neighborhood of their branching from ee and going to collision. The left branch can be obtained by reflexion with respect to the origin.

Another important family is the e–family which is stable for large positive values of c_H, h going to 0. The trajectory of our Moon [1] belongs to this family with $c_H = 6.54034$ and $0.016769 < x < 0.18717$, which is to the right of our figure. This family, as already seen in section 3.2, changes its stability through a pitchfork bifurcation at $c_H = 4.4999874$ ($h = 0.0523785$), that is, the bifurcated orbits have periods near the period of the original orbit. The unstable bifurcated branch, *ei*, can be continued to collision as c_H goes to $-\infty$.

We show the two stable bifurcated branches, *ee*, which after becoming unstable originate what we called the *e'i*–family. Again, to give an idea of the span, we have plotted the left most intersection with the x axis for each branch. To get the other intersection it is sufficient to take the negative value of the other branch. In Figure 10 we show some of the orbits belonging to the right branch, from a neighborhood of the change of stability up to a neighborhood of the colision. The left branch can be obtained by symmetry. So, we have two orbits which go to collision at the same energy value. Both of them can be continued after collision but they have perpendicular velocity again only after the second crossing of the x–axis, i.e., they are double–periodic. However, in the LC variables these orbits can still be found only after $T/2$, as before, because of the doubling of angles induced by the LC transformation. In fact they can be continued to a second asymptotical collision as c_H goes to $-\infty$. The x axis crossing, which has collided before the se orbits become double–periodic, goes away from the secondary, and it is the other crossing which goes to the asymptotical collision, as shown in Figure 9.

Note that the main bifurcations occur in the vicinity of the opening of the *zvc*.

Finally, there is the *er*–family which is stable throughout the c_H range (except, of course, at the 1 to 3 resonances). It was seen as the fixed point on the left of the Poincaré sections shown in Figures 4 and 7. This orbit, together with the change of topology of the invariant manifolds of the Lyapunov periodic orbits, is responsible for the persistent KAM structure. This will be discussed in the next section.

5. Globalization of the W^u and W^s of the Lyapunov orbits

In order to have a less cumbersome notation we make $(Q_1, Q_2, P_1, P_2) = (x, y, p_x, p_y)$. In the Poincaré section, Σ, defined by $y = 0$ $(H = h,\ p_y > 0)$, the periodic orbit is a fixed point with coordinates $(x, 0)$. From the time corrected monodromy matrix $\mathbf{M}$ we compute $D_{\mathbf{z}}\mathcal{P}(x, p_x)$ $(\mathbf{z} = (x, p_x))$, the differential of the Poincaré map.

The eigenvector, $\mathbf{v}_u$, associated to the eigenvalue $\lambda_u > 1$ of the differential of the Poincaré map, is tangent in the section to $W^U_{p.o.} \cap y = 0$, i.e., the section of the unstable manifold. This allows us to take, simply, a linear approximation of $W^U_{p.o.}$. We take a segment in the direction of $\mathbf{v}_u$ given by $\mathbf{z} + \varepsilon \mathbf{v}_u$, where $\varepsilon = \varepsilon_0 \exp(-p \log \lambda_s)$, $\quad p \in [0, 1)$. When p runs on $[0, 1)$ we cover a fundamental domain of $W^U_{p.o.} \cap y = 0$. This will ensure a suitably spaced image of this domain. These initial conditions on the fundamental domain are then propagated numerically by integrating the Hamiltonian equations. This generates a numerical approximation of $W^U_{p.o.}$. We shall refer to this procedure as numerical globalization of invariant manifolds. Then we make the desired Poincaré section which does not have to be the same used in the determination of the periodic orbit.

The symmetry S_2, given by the second equation (16), together with the symmetries implied by the double covering of the Levi–Civita regularization can be summarized as follows.

$$
\begin{array}{llll}
g_1 & (x, y, p_x, p_y, t) & Section : (y = 0, p_y > 0) & W^U_{L_1} \\
g_2 & (-x, y, p_x, -p_y, -t) & Section : (y = 0, p_y < 0) & W^S_{L_1'} \\
g_3 & (y, x, -p_y, -p_x, -t) & Section : (x = 0, p_x < 0) & W^S_{L_2} \\
g_4 & (-y, x, -p_y, p_x, t) & Section : (x = 0, p_x > 0) & W^U_{L_2}
\end{array}
$$

g_5	$(y, -x, p_y, -p_x, t)$	$Section : (x = 0, p_x < 0)$	$W^U_{L'_2}$
g_6	$(-y, -x, p_y, p_x, -t)$	$Section : (x = 0, p_x > 0)$	$W^S_{L'_2}$
g_7	$(x, -y, -p_x, p_y, -t)$	$Section : (y = 0, p_y > 0)$	$W^S_{L_1}$
g_8	$(-x, -y, -p_x, -p_y, t)$	$Section : (y = 0, p_y < 0)$	$W^U_{L'_1}$

This table has been constructed taking as generators g_2 and g_3. So, we can make four sections each turn of the orbits starting in the fundamental interval described above for a Lyapunov orbit of L_1. Then, we automatically allocate each crossing to its corresponding turn of the manifold obtained with the help of the above table. Each crossing can then be reverted to the physical space by the Levi–Civita transformation, if desired. In such case we have only two fixed points and four invariant manifolds (see Figure 3). Two examples of unstable manifolds are shown in Figure 11 in physical and in Levi–Civita variables. In Figure 11–b we show an unstable manifold which passes through collision.

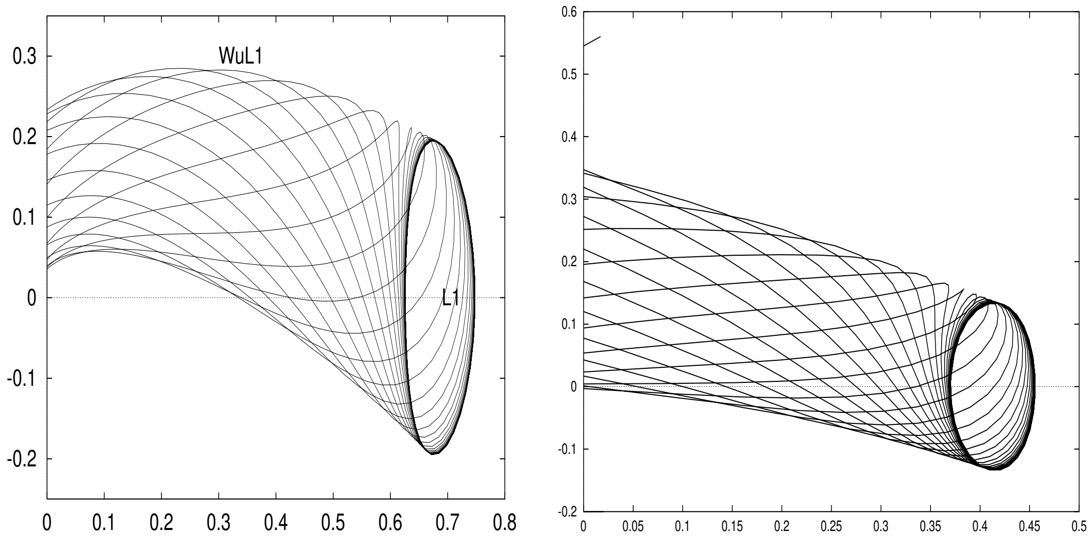

Figure 11. Left: Unstable manifold to a Lyapunov orbit around L_1 (physical variables) with initial condition $x = 0.6265940$. Note that it is fairly far from collision as it passes first near the Earth. Right: The collision unstable manifold (LC variables, $h = 0.07033103$) up to the first collision. Its Poincaré section is shown in Figure 15–e.

In Figure 12 we show 10 cuts through the section $y = 0$ for a small Lyapunov orbit around L_1 at $x = \pm 0.69192741$ with $h = 0.055562528$ ($c_H = 4.32638673$). The homoclinic cuts of $W^U_{p.o.}$ and $W^S_{p.o.}$ of L_1 and L_2 are shown in Figures 12–a and 12–b, respectively. Note that there is no homoclinic crossing in the first four cuts in either case, which have similar characteristics due to the symmetry above. Figure 12–c shows the heteroclinic crossings. They start earlier than the previous cases, more precisely at the second cut. We note that the cut labeled 1 near the x–axis is a local cut of the stable and unstable manifolds of L_1, as long as the same label means the first passage of the L_2 manifolds through the section. Finally, in Figure 12–d we exhibit 20 cuts of the four manifolds together with the two KAM islands at the center and the outward KAM structure. By doubling the number of cuts we can see that the cuts of the stable/unstable manifolds have covered a larger area. Three cuts of each of the eight original manifolds in LC variables, from which Figure

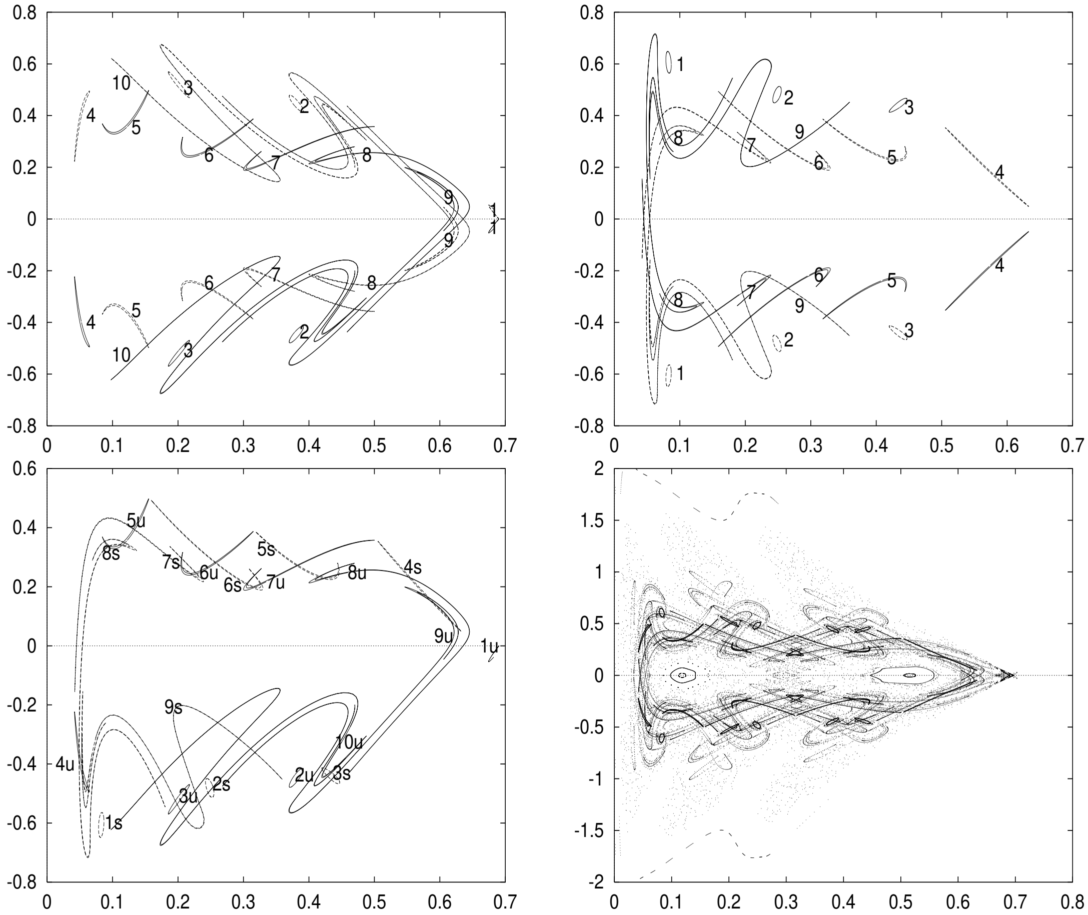

Figure 12. Poincaré section $y = 0$ of the stable (dashed line) unstable (continuous line) manifolds of periodic orbits around L_1 and L_2: $c_H = 4.32639940$ ($h = 0.055562284$) at $x = \pm 0.69192741$, respectively. From left to right, top to bottom: a) 10 cuts (1 local cut) showing the homoclinic points of the p.o. of L_1; b) same as a) for a p.o. around L_2, (1: first non–local cut); c) the heteroclinic points; d) the union of the 4 manifolds (number of cuts just doubled) plus part of the nearby KAM structure.

12 is originated, are displayed in Figure 13. The Lyapunov orbits have been labelled 1 to 4, corresponding to the neighborhood of L_1, L_2, L_1' and L_2', respectively. This is the first number shown in the label, followed by either "s" or "u", and the number of the cut. Again, as it can be noticed, cut number 1 is the local cut of the stable and unstable manifolds of the Lyapunov orbit around L_1.

Figures 14–a and 14–b show the same Poincaré section in physical and Levi–Civita variables, respectively, for $h = 0.05710310$ ($c_H = 4.2482189$). We show direct trajectories only. It is clear that apart from making the computation near collision possible, the regularizing variables deforms the orbits in a suitable way.

In Figure 15–a to 15–f we show the evolution of these cuts together with the KAM structure. As expected and already shown in Figures 12–a to 12–c, the cuts of the stable and unstable manifolds become thiner and longer the higher the number of the cut. Also, as the energy, h, grows (decreasing c_H) the first cuts becomes larger and larger and finally intercept each other. When we say the first cut, we mean the first non–local cut as in

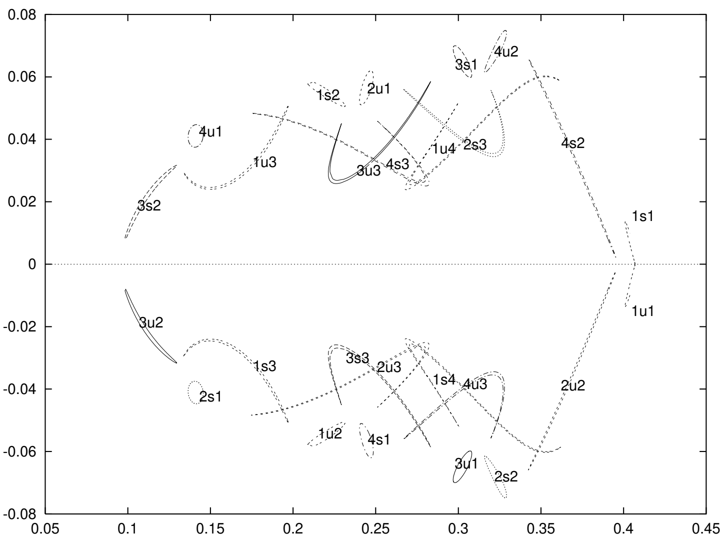

Figure 13. Three cuts of the eight manifolds which originated Figure 12. The first number refers to the manifold while the second refer to the section.

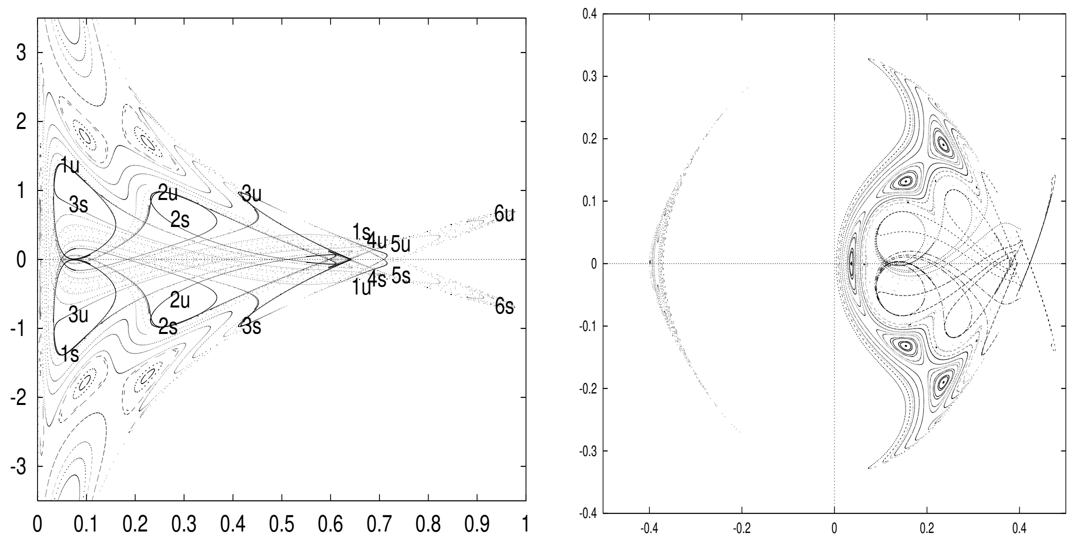

Figure 14. Invariant manifolds for $c_H = 4.2482189$ ($h = 0.05710310$), left to right: a) In physical variables there are six cuts of the unstable and stable manifolds; b) In Levi–Civita variables the twenty four cuts are to be distribute now among eight manifolds.

Figure 12. However, all the structure of cuts remains on the right of the main subsisting KAM structure, up to a certain energy value, filling the maple–leaf shaped stochastic zone. Some typical examples are shown in Figure 15–a to 15–d.

In fact for low values of the energy, the invariant stable and unstable manifolds of the Lyapunov periodic orbits are not responsible for this stochasticity since it appears before the *zvc* open (see Figure 4). There are other mechanisms to produce it, mainly the invariant manifolds of the periodic orbits of the e–family, after the pitchfork bifurcation. However, we note some key facts. When the unstable/stable manifolds pass through collision a change

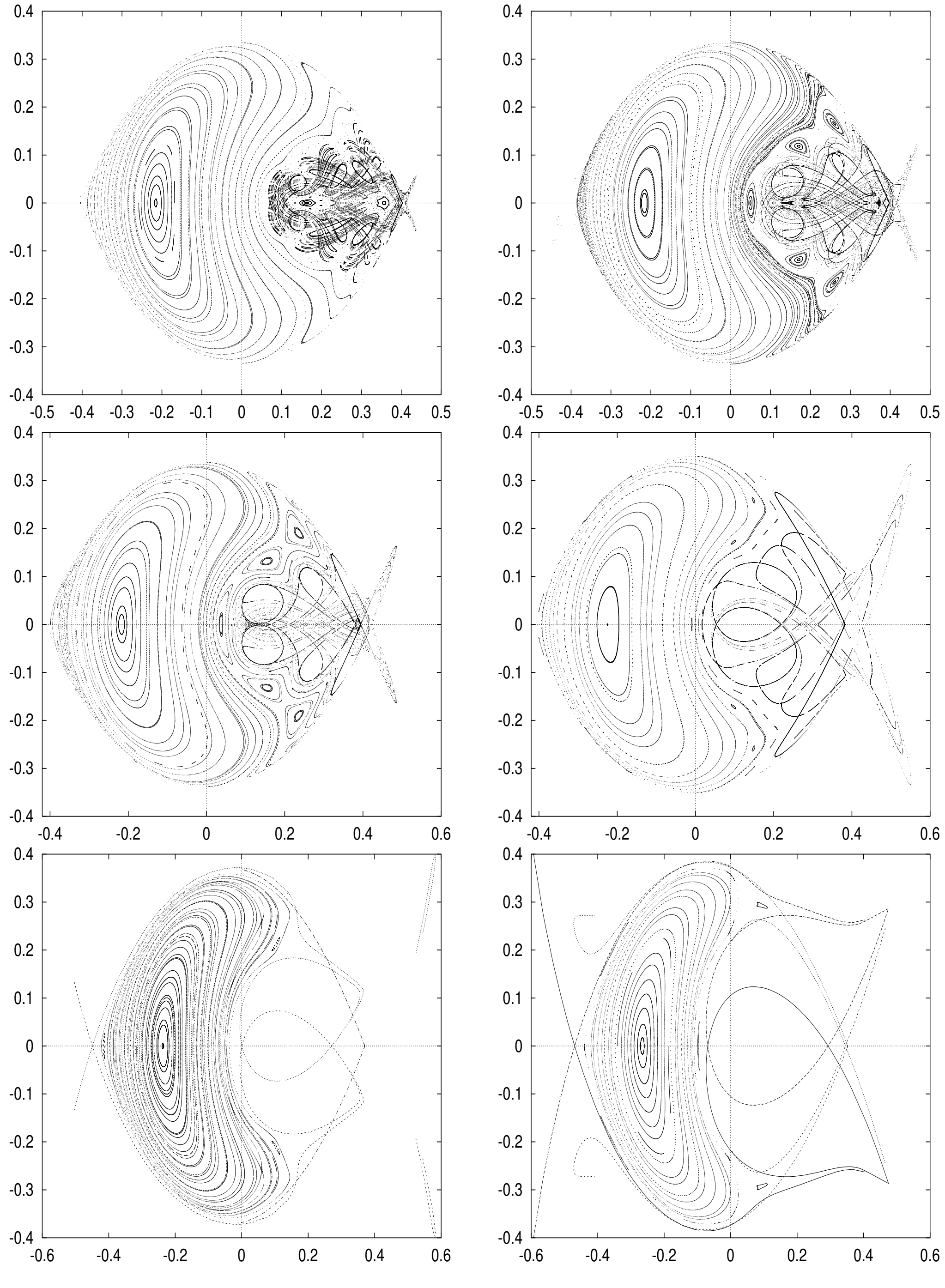

Figure 15. The invariant manifolds in Levi–Civita variables. From left to right, top to bottom: a) $h = 0.0557838$: the chaotic zone is gradualy filled by the cuts; b) $h = 0.05640708$: the cuts make way for the islands; c) $h = 0.05704225$; d) $h = 0.06157219$; e) $h = 0.07033103$: the cuts of the unstable/stable manifolds change when they pass through collision; they now surround the KAM retrograde structure; f) $h = 0.09305603$, after collision of the invariant manifold with the secondary.

of topology occurs. The cuts start going over to the left side of the Poincaré section and embrace the whole remaining KAM tori. This occurs precisely at $h = 0.07033103$, Figure 15–e, and the unstable manifold up to the first collision is the one shown in Figure 11–b. Note that the second cut of the manifolds, the tongue shaped cut grows a lobe which finally goes to the lefthand side of the section at the collision transition. In Figure 15–f we show the manifolds of a Lyapunov orbit past collision for $h = 0.09305603$, where the confinement of the remaining KAM tori by the unstable and stable manifolds is seen to persist. As a matter of fact, even when the energy value is small, some of the KAM structure is already confined by these manifolds. We mean the islands which are born with the pitchfork bifurcation which remains even when the *zvc* open till they are finally "squeezed" by the Lyapunov orbits manifolds.

Another interesting fact is shown in Figures 15–b and 15–c. The stochastic zone gets reorganized again and some islands appear. The unstable/unstable manifolds must undergo a topological change to "make room" for them. In fact, we think that some further work on these features could be worthwhile.

6. Final Comments

The stable/unstable manifolds of the Lyapunov family of periodic orbits form the corresponding manifolds of the full center manifold around the collinear libration points. As $W^U(W^C_{L_j})$ and $W^S(W^C_{L_j})$ are 3–dimensional, they have codimension 1 and, hence, they can act as *local confiners* for the motion. They are not responsible for the initial destruction of the KAM structure, which is clearly visible before the *zvc* open, and which is mainly due to the invariant manifolds of e–family of periodic orbits (direct "Moon–like orbits" after instabilization). From the moment when the invariant manifolds are born with the Lyapunov periodic orbits (when the *zvc* open) they already know that they should exhibit homoclinic and heteroclinic phenomena. Furthermore, when the stochastic zone gets organized due to some multifurcation the stable/unstable manifolds have to acommodate themselves to that fact, i.e, they have to make room for the islands. The manifolds which reach the secondary for the first time, are seen to play a key role.

Acknowledgements

The first author has been supported by DGICYT grant PB 94-0215 (Spain). He is also pleased to acknowledge partial support of the EC grant ERBCHRXCT940460, and the catalan grant CIRIT 1996S0GR-00105. A stay of the second author in Barcelona was possible thanks to a CNPq grant 201612/93.8.

References

1. Hénon, H.: Numerical Stability of the Restricted Problem: V. Hill's Case: Periodic Orbits and their Stability, *Astron. Astrophys.* **1**, (l969), 223–238.
2. Gómez, G., Llibre, J., Martínez, R. and Simó, C.: *Station Keeping of Libration Point Orbits.* ESOC Contract 5648/83/D/JS(SC), Final Report, 1985.
3. Simó, C.: Estabilitat de systems Hamiltonians, *Memorias de la Real Academia de Ciencias y Artes de Barcelona* **48**, (1989), 303–348.
4. Simó, C.: Analytical and numerical computation of invariant manifolds. In D. Benest et C. Froeschlé, editors, *Modern methods in celestial mechanics*, 285–330, Editions Frontières, 1990.
5. Stiefel E.L., Scheifele, G.: *Linear and Regular Celestial Mechanics*, Springer–Verlag (1971).
6. Szebehely, V.: *Theory of Orbits*, Academic Press (1967).